Inorganic Chemistry

Communication

pubs.acs.org/IC

Substituent-Dependent Spin-Density Distribution and Coexistence of Fe 3d and π Spins on Ferrocene−Tetrathiafulvalene Hybrids

Tetsuro Kusamoto,*[†] Hiroshi Nishihara,[†] and Reizo Kato[‡]

[†]Department of Chemistry, School of Science, The University of Tokyo, 7-3-1 Hongo, Bunkyo-ku, Tokyo 113-0033, Japan

[‡]RIKEN, 2-1 Hirosawa, Wako-shi, Saitama 351-0198, Japan

Supporting Information

ABSTRACT: Ferrocene (Fc) and tetrathiafulvalene (TTF) moieties were incorporated into novel hybrid molecules of structure $FcS_4TTF(R)_2$ (R = CF_3 and SMe). $[FcS_4TTF(R)_2]^{\bullet+}$ exhibited R-dependent spin-density distribution, and $[FcS_4TTF(CF_3)_2]^{\bullet\bullet 2+}$ showed the coexistence of Fc-centered Fe 3d and TTF-centered π spins. The solid-state molecular structures in different oxidation states reflect their characteristic spin states.

Electron donors, acceptors, and their hybrids are promising components of molecule-based functional materials and devices because the removal or addition of electrons (i.e., oxidation or reduction) enables fine control of the compounds' structures and their electronic and spin states.[1] For example, such properties are shown by ferrocene (Fc) and multisulfur π-conjugated molecules, such as tetrathiafulvalenes (TTFs) and metalladithiolenes. Fc forms localized 3d spin upon oxidation, and TTFs form delocalized π spin. The former behaves as a magnetic center, and the latter exhibits electrical (super)-conductivity in the solid state.[2,3] A combination of these two molecular systems, Fc−TTF, is expected to achieve novel magnetoconducting properties by multiple oxidation, which would lead to unusual electronic and spin states, such as the coexistence of 3d spins and π-conducting electrons in the same molecule. Many Fc−TTF and Fc−metalladithiolene hybrids have been prepared, and their multistep redox properties have been investigated by cyclic voltammetry;[4] however, the changes of their molecular and electronic structures and spin-density distribution, which are accompanied by the multistep redox behaviors, have not been fully investigated. This is partly due to the difficulty of isolating the chemically unstable species, such as highly oxidized dicationic compounds.

This work reports the successful isolation of the dicationic, monocationic, and neutral forms of new Fc−TTF hybrids $FcS_4TTF(R)_2$ (R = CF_3 and SMe; Chart 1). Structural and spectroscopic investigations showed that the molecular structure of each oxidation state reflects its spin-density distribution. Chemical modification on R significantly altered the spin-density distribution in the monocation. The dication showed the coexistence of localized 3d and delocalized π spins with antiferromagnetic spin−spin interaction.

Chart 1. Chemical Structures of Molecules

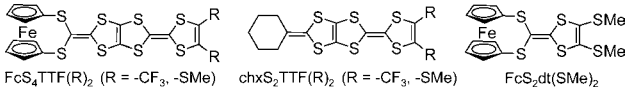

$FcS_4TTF(R)_2$ samples were prepared according to Scheme S1 in the Supporting Information (SI).

The electrochemical properties of the complexes were investigated by cyclic voltammetry. $FcS_4TTF(SMe)_2$ showed three reversible oxidation waves; $FcS_4TTF(CF_3)_2$ showed two (Figure 1a). These were attributed to the two electron-donating

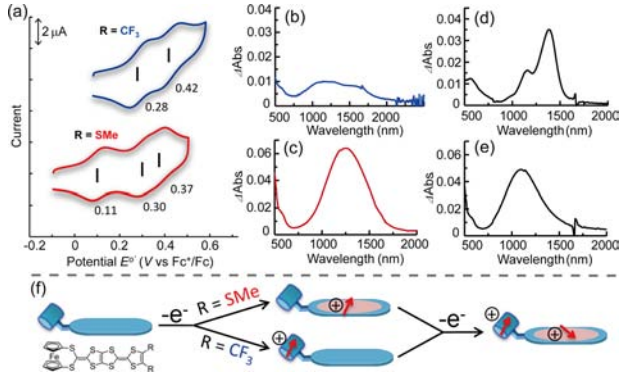

Figure 1. (a) Cyclic voltammograms of $FcS_4TTF(R)_2$ at 100 $mV \cdot s^{-1}$ in 0.1 M $Bu_4N \cdot ClO_4$−PhCN at room temperature. ΔAbs of (b) $FcS_4TTF(CF_3)_2$, (c) $FcS_4TTF(SMe)_2$, (d) $chxS_2TTF(CF_3)_2$, and (e) $chxS_2TTF(SMe)_2$. ΔAbs indicates the difference between the absorption spectra of the neutral and electrochemically generated $1e^-$-oxidized complexes. (f) Schematic oxidation behavior.

Fc moieties and the π-extended TTF (exTTF) moieties. The redox potentials were compared with those of related compounds (Table S1 in the SI). $FcS_4TTF(CF_3)_2$ showed a more positive first redox potential $E_1^{o/ox}$ (0.28 V vs Fc^+/Fc) than did $FcS_4TTF(SMe)_2$ (0.11 V); the value is close to that shown by $FcS_4dt(SMe)_2$ (0.26 V),[4a] indicating Fc-centered oxidation. The second redox potential $E_2^{o/ox}$ (0.42 V) was slightly more positive than the $E_1^{o/ox}$ value of EDT-$TTF(CF_3)_2$ (0.37 V), suggesting that the second oxidation was centered on the exTTF moiety. $FcS_4TTF(SMe)_2$ showed an $E_1^{o/ox}$ value similar to that of $E_1^{o/ox}$ of EDT-$TTF(SMe)_2$ (0.10 V) and an $E_2^{o/ox}$ (0.30 V) value similar to that of $E_1^{o/ox}$ of $FcS_4dt(SMe)_2$. This suggests that the first and second oxidation processes of $FcS_4TTF(SMe)_2$ were due to the exTTF and Fc moieties, respectively.[5] The expected

Received: September 5, 2013
Published: November 26, 2013

redox behavior of $FcS_4TTF(R)_2$ (Figure 1f) was confirmed by electrochemical vis−near-IR absorption spectroscopy.

Differential absorption spectra (ΔAbs), which indicate the difference between the absorption spectra of the neutral and electrochemically generated $1e^-$-oxidized complexes, were obtained for $FcS_4TTF(R)_2$ and the reference complexes $chxS_2TTF(R)_2$ (R = CF_3 and SMe; Figure 1b−e), which contain a cyclohexane skeleton (chx) in place of the Fc unit. ΔAbs of $FcS_4TTF(SMe)_2$ displayed a strong absorption band in the vis−near-IR region that is closely similar to ΔAbs of $chxS_2TTF(SMe)_2$; therefore, the absorption band is assigned to a $\pi-\pi^*$ transition centered on the exTTF moiety.[6] This result suggests that oxidation of the exTTF moiety is the first oxidation process in $FcS_4TTF(SMe)_2$. ΔAbs of $FcS_4TTF(CF_3)_2$ showed broad absorption in the range 750−2000 nm. The spectrum differs from that of $chxS_2TTF(CF_3)_2$, which displayed a strong $\pi-\pi^*$ absorption band at 1000−1800 nm,[6] but is similar to that of $[FcS_4dt(SMe)_2]^{\bullet+}$.[4a] The Fc moiety in $[FcS_4dt(SMe)_2]^{\bullet+}$ was oxidized to Fc^+, indicating that the oxidation occurred mainly at the Fc moiety in $FcS_4TTF(CF_3)_2$.

Electrochemical analysis and absorption spectroscopy revealed that the reaction center of the first oxidation process depends on R (Figure 1f); specifically, the spin-density distribution of $[FcS_4TTF(R)_2]^{\bullet+}$ can be controlled by changing R, yielding localized 3d spin for R = CF_3 and delocalized π spin for R = SMe.

We next attempted to isolate $FcS_4TTF(R)_2$ in various oxidation states to elucidate whether the redox behavior established by the solution chemistry influences the solid-state molecular structure. Several experimental techniques were examined, and single crystals of a $[FcS_4TTF(SMe)_2]^{\bullet+}$ monocation salt, $[FcS_4TTF(SMe)_2][F_4TCNQ]$, were successfully prepared by reacting $FcS_4TTF(SMe)_2$ with F_4TCNQ in hot chlorobenzene.[7] Crystals of a $[FcS_4TTF(CF_3)_2]^{\bullet\bullet2+}$ dication salt, $[FcS_4TTF(CF_3)_2](BF_4)_2{\cdot}o\text{-}PhCl_2$, were prepared by electrochemical oxidation (1 μA in o-$PhCl_2$ at 293 K in the presence of $^nBu_4N{\cdot}BF_4$). Single crystals of neutral $FcS_4TTF(SMe)_2$ suitable for XRD analysis were obtained by recrystallization from hot chlorobenzene.[8]

A crystal of $FcS_4TTF(SMe)_2$ contains two crystallographically independent molecules, in which the exTTF skeleton of one molecule forms a bent structure (Figure 2a), as it does in neutral exTTFs.[9] The two cyclopentadienyl (Cp) rings are nearly parallel (178°); they also lie parallel to the molecular long axis of the exTTF moiety. The Cp−Cp interplanar distance (3.29 Å) within the molecule is comparable to the distance between the two sulfur atoms along the molecular short axis in the exTTF moiety (3.00 Å), suggesting that the Fc moiety does not disturb the intermolecular side-by-side interaction through the sulfur atoms. Indeed, several intermolecular S···S contacts shorter than the sum of the van der Waals radii of two sulfur atoms (3.6 Å) were observed along the side-by-side direction (Figure S1 in the SI).

The molecular structure of the $[FcS_4TTF(SMe)_2]^{\bullet+}$ monocation in the $[FcS_4TTF(SMe)_2][F_4TCNQ]$ crystal is displayed in Figure 2b. The monocation constructs a fairly planar exTTF skeleton, in contrast with the neutral $FcS_4TTF(SMe)_2$. The bond lengths of the exTTF moiety in the monocation differ from those of the neutral species; the differences reflect the highest occupied molecular orbital of $FcS_4TTF(SMe)_2$ calculated using density functional theory (DFT), in which the bonding C−C double bonds are elongated and the antibonding C−S bonds are shortened by $1e^-$ oxidation (Table S3 in the SI). The Fc moiety

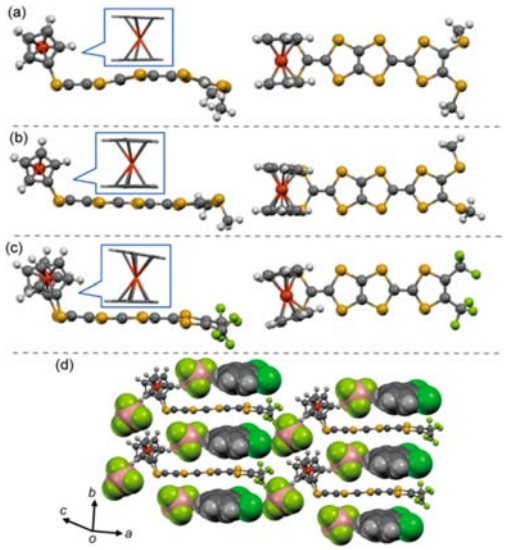

Figure 2. Molecular structures of (a) $FcS_4TTF(SMe)_2$, (b) $[FcS_4TTF(SMe)_2]^{\bullet+}$, and (c) $[FcS_4TTF(CF_3)_2]^{\bullet\bullet2+}$ in the solid state. Inset: structure of the Fc moiety (tube model). (d) Crystal structure of $[FcS_4TTF(CF_3)_2](BF_4)_2{\cdot}o\text{-}PhCl_2$. BF_4^- and o-$PhCl_2$ are shown as CPK models.

retains a similar structure after $1e^-$ oxidation. A comparison of the molecular structures shows that the oxidation of $FcS_4TTF(SMe)_2$ occurs at the exTTF moiety to form $[FcS_4TTF(SMe)_2]^{\bullet+}$ with π-radical nature. The increased C−S−C angle around the bridging sulfur atoms supports the exTTF-centered oxidation.[4a] $[FcS_4TTF(SMe)_2]^{\bullet+}$ and $[F_4TCNQ]^{\bullet-}$ are dimerized in the crystal and construct a one-dimensional stacking structure (Figure S2 in the SI). Several intradimer atomic contacts are detected in the dimers. The strong antiferromagnetic interaction within each dimer results in the singlet ground state, which was confirmed by superconducting quantum interference device (SQUID) measurements (Figure S3 in the SI).

$[FcS_4TTF(CF_3)_2]^{\bullet\bullet2+}$ forms a characteristic structure in the solid state. The π-conjugated dithiolene moiety is almost planar, except the terminal five-membered ring, which is tilted against the plane with a dihedral angle of 10° (Figure 2c). Such tilt was not observed in $FcS_4TTF(SMe)_2$ or $[FcS_4TTF(SMe)_2]^{\bullet+}$. This result evidences the oxidation of the exTTF moiety; the central C═C double bond has single-bond character, which allows the observed tilt. The C−C and C−S bonds in the exTTF moiety differ from those of neutral $FcS_4TTF(SMe)_2$, with a manner similar to that of $[FcS_4TTF(SMe)_2]^{\bullet+}$. The distinct structural character was shown by the Fc moiety. The two Cp rings are tilted at 8° to each other and are not parallel to the molecular long axis of the exTTF moiety. Such structural distortion was not observed in $FcS_4TTF(SMe)_2$ and the $[FcS_4TTF(SMe)_2]^{\bullet+}$ monocation, inferring that the Fc moiety was oxidized to paramagnetic ferrocenium in the dication. Namely, a π spin delocalized on the exTTF moiety and a Fe 3d spin located at the Fc moiety coexist in $[FcS_4TTF(CF_3)_2]^{\bullet\bullet2+}$. Among the many reported derivatives of Fc and TTF, such a diradical with two different kinds of spin has not previously been reported. The structural observations of $FcS_4TTF(R)_2$ in the different oxidation states (neutral, monocationic, and dicationic) revealed that the molecular structure reflects the spin-density distribution, corroborating expectations from the solution chemistry.

dx.doi.org/10.1021/ic4022678 | Inorg. Chem. 2013, 52, 13809−13811

Figure 2d shows $[FcS_4TTF(CF_3)_2]^{\bullet\bullet 2+}$ molecules surrounded by BF_4^- and *o*-$PhCl_2$ molecules and separated from each other in the crystal.[10] This allows evaluation of the intramolecular exchange interaction between the π and 3d spins via measurements of magnetic susceptibility.

The χT product of polycrystalline $[FcS_4TTF(CF_3)_2](BF_4)_2$·*o*-$PhCl_2$ under 1 T (Figure 3a) in the range of 70−300 K was

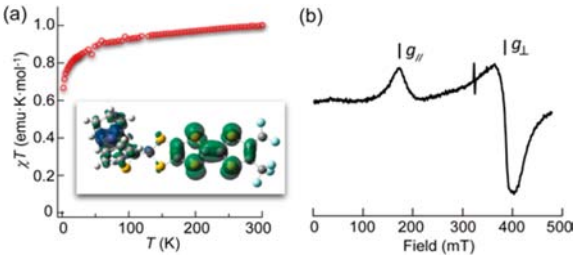

Figure 3. (a) Temperature-dependent χT of $[FcS_4TTF(CF_3)_2](BF_4)_2$·*o*-$PhCl_2$ at 1 T. Inset: calculated spin-density distribution (blue, α spin; green, β spin) of $[FcS_4TTF(CF_3)_2]^{\bullet\bullet 2+}$ under a broken-symmetry singlet state. (b) EPR spectrum of $[FcS_4TTF(CF_3)_2](BF_4)_2$·*o*-$PhCl_2$ measured at 15 K. $g_\parallel$ and $g_\perp$ are 3.78 and 1.70, respectively. Note the small impurity signal at 336 mT.

analyzed using a singlet−triplet model ($\mathcal{H} = 2J\sum S_{Fc}\cdot S_{TTF}$)[11,12] to afford a Curie constant (C) of 1.01 emu·K·mol^{-1} with a g value of 2.23 and an exchange interaction parameter J/k_B of −6.0 K. The C value was higher than the value (0.75 emu·K·mol^{-1}) expected for two noninteracting $S = {}^1/_2$ spins with $g = 2$, suggesting the diradical character with 3d and π spins. The negative J value indicates a dominant intramolecular antiferromagnetic interaction between the two spins. This magnetic situation is qualitatively supported by the spin-density distribution calculated on the basis of the broken-symmetry DFT method; the spins coexist on the iron ion and on the TTF moiety with antiferromagnetic spin alignment.[13] The electron paramagnetic resonance (EPR) spectrum of polycrystalline $[FcS_4TTF(CF_3)_2](BF_4)_2$·*o*-$PhCl_2$ at 5 K displays a highly anisotropic signal with an axial character, similar to $[FcS_4dt\text{-}(Me)_2]^{\bullet+}$.[4a] This result supports the existence of the Fe 3d spin that interacts with the π spin (Figure 3b). The through-bond intramolecular magnetic interaction is affected by the structure of the molecule because the structure determines the degree of orthogonality or overlap between the two noncanonical π and 3d spin orbitals.

In conclusion, $FcS_4TTF(R)_2$ demonstrated R-dependent redox behavior and spin-density distribution. The solid-state molecular structures in different oxidation states reflect the molecules' spin centers. $[FcS_4TTF(CF_3)_2]^{\bullet\bullet 2+}$ showed simultaneously both 3d and π spins within one molecule. Unpaired π electrons can form metallic bands in the solid state, and the interaction between the 3d spins and the π-conducting electrons can produce unusual magnetoconducting properties, as observed in magnetic molecular conductors.[3] $FcS_4TTF(R)_2$, which would be expected to show through-bond π−d interactions, is a promising candidate for the development of novel molecular materials, in which magnetism and conductivity correlate strongly with each other.

■ ASSOCIATED CONTENT

Ⓢ Supporting Information

Details of DFT calculations, redox potential, bond lengths, crystallographic data, synthetic scheme and procedures, χ of $[FcS_4TTF(SMe)_2][F_4TCNQ]$, and X-ray crystallographic files in CIF format. This material is available free of charge via the Internet at http://pubs.acs.org.

■ AUTHOR INFORMATION

Corresponding Author

*E-mail: kusamoto@chem.s.u-tokyo.ac.jp.

Notes

The authors declare no competing financial interest.

■ ACKNOWLEDGMENTS

This research was supported by Grants-in-Aid from MEXT of Japan (Grants 22224006 and 24750142).

■ REFERENCES

(1) (a) Saito, G.; Yoshida, Y. *Bull. Chem. Soc. Jpn.* **2007**, *80*, 1−137. (b) Day, P.; Kurmoo, M. *J. Mater. Chem.* **1997**, *7*, 1291−1295. (c) Kusamoto, T.; Kume, S.; Nishihara, H. *J. Am. Chem. Soc.* **2008**, *130*, 13844−13845. (d) Kusamoto, T.; Kume, S.; Nishihara, H. *Angew. Chem., Int. Ed.* **2010**, *49*, 529−531.

(2) Miller, J. S.; Calabrese, J. C.; Rommelmann, H.; Chittipeddi, S. R.; Zhang, J. H.; Reiff, W. M.; Epstein, A. J. *J. Am. Chem. Soc.* **1987**, *109*, 769−781.

(3) Special issue on Molecular Conductors: *Chem. Rev.* **2004**, *104*, 4887−5782.

(4) (a) Kusamoto, T.; Takada, K.; Sakamoto, R.; Kume, S.; Nishihara, H. *Inorg. Chem.* **2012**, *51*, 12102−12113. (b) Wilkes, S. B.; Butler, I. R.; Underhill, A. E.; Hursthouse, M. B.; Hibbs, D. E.; Malik, K. M. A. *J. Chem. Soc., Dalton Trans.* **1995**, 897−903. (c) Wilkes, S. B.; Butler, I. R.; Underhill, A. E.; Kobayashi, A.; Kobayashi, H. *J. Chem. Soc., Chem. Commun.* **1994**, 53−54. (d) Lee, H.-J.; Noh, D.-Y. *J. Mater. Chem.* **2000**, *10*, 2167−2172. (e) Mueller-Westerhoff, U. T.; Sanders, R. W. *Organometallics* **2003**, *22*, 4778−4782. (f) Iyoda, M.; Takano, T.; Otani, N.; Ugawa, K.; Yoshida, M.; Matsuyama, H.; Kuwatani, Y. *Chem. Lett.* **2001**, *30*, 1310−1311. (g) Lee, H.-J.; Noh, D.-Y.; Underhill, A. E.; Lee, C.-S. *J. Mater. Chem.* **1999**, *9*, 2359−2363. (h) Skabara, P. J.; Bryce, M. R.; Batsanov, A. S.; Howard, J. A. K. *J. Org. Chem.* **1995**, *60*, 4644−4646. (i) Andreu, R.; Garin, J.; Orduna, J.; Saviron, M.; Uriel, S. *Synth. Met.* **1995**, *70*, 1113−1114. (j) Moore, A. J.; Skabara, P. J.; Bryce, M. R.; Batsanov, A. S.; Howard, J. A. K.; Daley, S. T. A. K. *J. Chem. Soc., Chem. Commun.* **1993**, 417−419.

(5) Third oxidation processes are attributed to the TTF moieties. This expectation is supported by the similarity between $\Delta E^{o\prime}{}_{EDT\text{-}TTF(SMe)_2}$ ($=E_2^{o\prime ox} - E_1^{o\prime ox} = 0.25$ V) and $\Delta E^{o\prime}{}_{FcS4TTF(SMe)_2}$ ($=E_3^{o\prime ox} - E_1^{o\prime ox} = 0.26$ V).

(6) $chxS_2TTF(R)_2$ does not include the Fc moiety; it shows a TTF-centered π−π^* transition upon 1e$^-$ oxidation.

(7) Monoanionic F_4TCNQ was confirmed by the appearance of a peak at $\nu_{CN} = 2192$ cm^{-1} in Fourier transform infrared spectroscopy, which also indicates the monocationic state of $FcS_4TTF(SMe)_2$: Meneghetti, M.; Pecile, C. *J. Chem. Phys.* **1986**, *84*, 4149−4162 We note that the single crystal of the $[FcS_4TTF(CF_3)_2]^{\bullet+}$ monocation salt was not obtained in spite of much effort on our part.

(8) Crystallographic data were summarized in Table S2 in the SI.

(9) Misaki, Y. *Sci. Technol. Adv. Mater.* **2009**, *10*, 024301−22.

(10) *o*-$PhCl_2$ is disordered in three positions, which are not shown for clarity. One intermolecular S···S contact mediated through bridging sulfur atoms and one S···C contact were found.

(11) At low temperature, several magnetic contributions such as spin−orbit coupling on the Fe 3d spin and intermolecular magnetic interaction can be present, which hinder the magnetic contribution from the intramolecular exchange interaction.

(12) Kahn, O. *Molecular Magnetism*; Wiley-VCH: New York, 1993.

(13) For details, see the SI.